Validation of High Density Electrode Arrays for Cochlear Implants: A Computational and Structural Approach

A Dissertation
Presented to
The Academic Faculty

By

Jessica D. Falcone

In partial fulfillment
of the requirements for the degree
Master of Science in the
School of Electrical and Computer Engineering

Georgia Institute of Technology
May 2011

Validation of High Density Electrode Arrays for Cochlear Implants:
A Computational and Structural Approach

Approved by:

Dr. Pamela T. Bhatti, Advisor
College of Electrical and Computer Engineering
Georgia Institute of Technology

Dr. Robert J. Butera
College of Electrical and Computer Engineering
Georgia Institute of Technology

Dr. Gregory D. Durgin
College of Electrical and Computer Engineering
Georgia Institute of Technology

Date Approved: March 29th, 2011

ACKNOWLEDGMENTS

Partial support of this research was provided by the Woodrow W. Everett, Jr. SCEEE Development Fund in cooperation with the Southeastern Association of Electrical and Computer Engineering Department Heads.

In addition to the dissertation committee, the following individuals are acknowledged for their contribution in supporting the completion of this Master's thesis: Dr. Brian J. McKinnon and Dr. Kenneth Iverson from the Department of Otolaryngology at the Medical College of Georgia.

TABLE OF CONTENTS

LIST OF TABLES

LIST OF FIGURES

SUMMARY

Creating high resolution, or high-density, electrode arrays may be the key for improving cochlear implant users' speech perception in noise, comprehension of lexical languages, and music appreciation. Contemporary electrode arrays use multipolar stimulation techniques such as current steering (shifting the spread of neural excitation in between two physical electrodes) and current focusing (narrowing of the neural spread of excitation) to increase resolution and more specifically target the neural population. Another approach to increasing resolution incorporates microelectromechanical systems (MEMS) fabrication to create a thin film microelectrode (TFM) array with a series of high density electrodes. Validating the benefits of high density electrode arrays requires a systems-level approach. This hypothesis will be tested computationally via cochlea and auditory nerve simulations, and in vitro studies will provide structural proof-of-concept.

By employing Rattay's activating function and entering it into Litvak's neural probability model, a first order estimation model was obtained of the auditory nerve's response to electrical stimulation. Two different stimulation scenarios were evaluated: current steering vs. a high density electrode and current focusing of contemporary electrodes vs. current focusing of high density electrodes. The results revealed that a high density electrode is more localized than current steering and requires less current. A second order estimation model was also created COMSOL, which provided the resulting potential and current flow when the electrodes were electrically stimulated. The structural tests were conducted to provide a proof of concept for the TFM arrays' ability to contour to the shape of the cochlea. The TFM arrays were integrated with a standard insertion platform (IP), and in vitro tests were performed on human cadaver cochleae. Post analysis histology was conducted on the specimens. Only three of the ten implanted TFM/IPs suffered severe delamination. This statistic for scala vestibuli excursion is not an outlier when compared to previous data recorded for contemporary cochlear electrode arrays.

CHAPTER 1
INTRODUCTION

Cochlear implants are neurodevices that electrically stimulate the auditory nerve and restore hearing to the deaf. Over 219,000 people worldwide have been implanted with a cochlear prosthesis, and of that number, 71,000 people are in the United States [1]. Despite drastic improvements over the past few decades, current cochlear implant users still experience difficulty with understanding speech in noise, lexical tonal language (i.e. Mandarin) comprehension, and music appreciation. One solution to improving hearing is to increase the resolution, or number of electrodes, on the cochlear implant array. Contemporary electrode arrays have between 12 and 22 stimulating sites [2]. However, size restrictions due to electrode manufacturing and the physical dimensions of the cochlea prevent this number from increasing. To compensate for the lack of high resolution, techniques such as current focusing and current steering were developed. Current focusing precisely stimulates neural populations, and current steering stimulates neural populations between two electrodes. Another approach to increasing resolution incorporates microelectromechanical systems (MEMS) fabrication to create a thin film microelectrode (TFM) array with a series of high density electrodes [3]. Developing a high density electrode array may be the key to improving hearing for cochlear implant users.

While both current focusing and current steering allow for greater control of neural stimulation, it is hypothesized that the electrical spread of high density electrodes will be significantly narrower and require less current than the contemporary electrode counterpart. Validating the benefits of high density electrode arrays requires a systems-level approach. This hypothesis will be tested computationally via cochlea and auditory nerve simulations, and in vitro studies will provide structural proof-of-concept. The cochlea and auditory nerve simulations will be composed of a first order estimate model using the activating function and neural firing probability model. The second order estimation will

be produced in COMSOL, a finite element method modeling software. The in vitro structural experiments will be conducted using a novel integration of the TFM arrays with a standard surgical insertion platform. The arrays will be inserted into cadaver cochleae that have been removed from the temporal bone, and histological analysis will be performed.

CHAPTER 2

BACKGROUND

Cochlear implants provide neural stimulation to restore auditory response to people with sensorineural hearing loss. Section 2.1 reviews the basic mechanisms of hearing and the functionality of cochlear implants. Section 2.1.1 explains the different types of multipolar stimulation with the cochlear electrode array. Section 2.1.2 highlights the state-of-art features between the major cochlear implant companies.

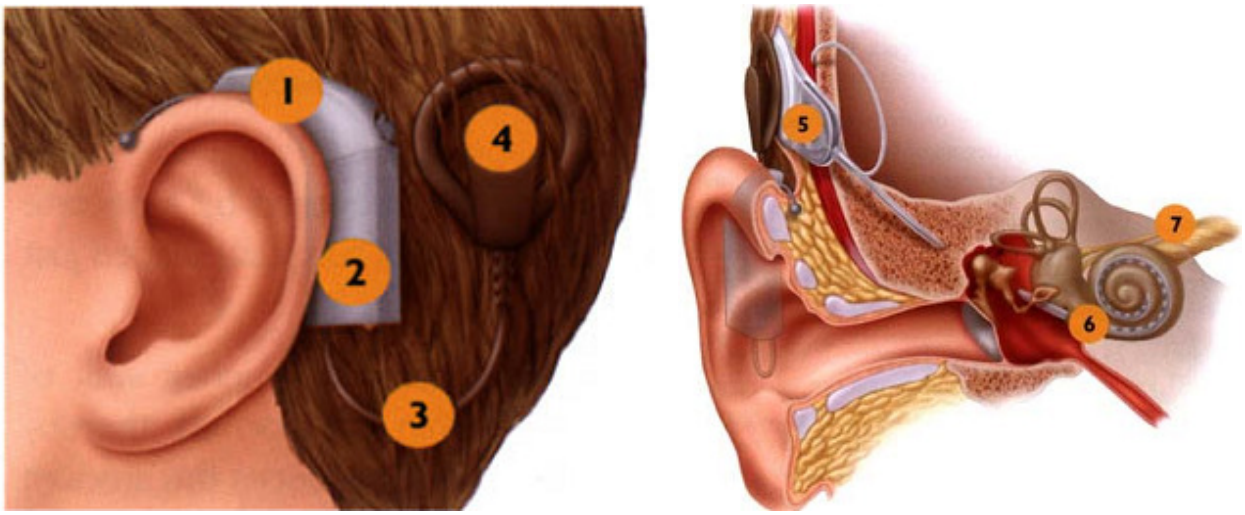

Figure 2.1 – Diagram of cochlear implant components: (1) Signal Processor, (2) Battery, (3) Connector, (4) External RF Transmitter, (5) Internal RF Receiver and Stimulator, (6) Electrode Array, and (7) Vestibulocochlear nerve. *Images courtesy of Citizen Airman.*

2.1 Overview of Cochlear Implants

The ear is divided into three parts: outer, middle and inner. The cochlea, a fluid-filled membrane, is located in the inner ear. During the process of normal hearing, the outer ear captures sound, which travels to the ear drum in the middle ear and is converted into mechanical vibrations. These vibrations pass through the ossicles, three small bones located in the middle ear. Next the vibrations travel into the cochlea in the inner ear, and fluid displacement reveals the frequency information of the acoustic signal. The cochlea is tonotopically organized, which means that high

frequencies activate the base and low frequencies activate the apex. Attached to the cochlea are small hair cells that bend when the cochlea experiences displacement. When bent, these hair cells activate auditory nerve fibers, which send signals to the brain relaying acoustic information [4].

Sensorineural deafness is caused by the disruption of this hearing process. In the majority of the cases, it is the hair cells that are damaged, not the auditory nerve fibers. A cochlear implant functions by directly stimulating the auditory nerves through speech processing. The cochlear implant is composed of several parts. First, sound travels through the microphone and into the signal processer, both of which are located in an external earpiece. The processed signal then travels to an external RF transmitter which is magnetically attached to the head. The signal is transmitted inside the body to the RF receiver and stimulator. The signal is converted into pulses and sent to the electrode array in the cochlea for stimulation of the auditory nerve fibers. **Figure 2.1** illustrates the anatomical positioning of the cochlear implant [4].

2.1.1 State of the Art

Table 2.1 outlines the current cochlear implant systems on the market. Included are the Harmony™ HiResolution™ Bionic Ear System (Advanced Bionics, Sylmar, CA), the Cochlear™ Nucleus®5 System (Cochlear Ltd., Sydney, Australia), the MAESTRO™ Cochlear Implant System (MED-EL, Innsbruck, Austria), and the Saphr® + Digisonic® SP (MxM – Neurelec, Vallauris, France). For each company, all electrodes are made of platinum. Cochlear Ltd.'s Nucleus CI512 has the largest number of electrodes (22) and Advanced Bionics' HiFocus Helix has the smallest electrode midpoint spacing (0.85 mm). Both Cochlear Ltd. and Advanced Bionics offer bipolar stimulation. Advanced Bionics is the only company to offer current steering with their HiRes with Fidelty 120 speech processor. Advanced Bionics claims that through current steering, the number of stimulation channels increases from 16 to 120 [5 - 9].

Table 2.1 – State-of-the-art systems marketed by cochlear implant companies

	Advanced Bionics	Cochlear Ltd.	MED-EL	MxM - Neurelec
Cochlear Implant System	*Harmony™ HiResolution™*	*Nucleus® 5*	*MAESTRO™*	*Saphyr® + Digisonic® SP*
Electrode Array	*HiFocus® Helix*	*Nucleus CI512*	*SONATA TI 100 PULSAR CI 100*	*Digisonic® SP*
# of Channels	16	22	12	20
Electrode Midpoint Spacing (mm)	0.85	0.9 - 1.6	2.4	1.2
Electrode Diameter (mm)	0.7 - 1.2	0.5 - 0.8	0.5 - 1.3	0.5 - 1.07
Active Electrode Array Length (mm)	13	15	32	25
Speech Processor	*HiRes with Fidelity™ 120*	*Nucleus CP810*	*Opus 2*	*Saphyr®*
Bipolar Stimulation	Yes	Yes	No	No
Current Steering	Yes	No	No	No

2.1.2 Simultaneous Multipolar Stimulation

The two common multipolar stimulation techniques in cochlear implants are current steering and current focusing. Current steering requires the simultaneous stimulation of two physical electrodes by weighted currents. The summation of the electrical fields stimulates nerves located between the two physical electrodes which are not normally activated by a single electrode (**Figure 2.2 A-B**). This results in cochlear implant patients hearing an intermediary pitch precept. Current steering is measured in terms of α, which represents the weighted current of the second electrode [10, 11, 12]. Current focusing requires three electrodes, where a positive current is applied to the central electrode and a certain percentage of negative current is applied to the two side electrodes. The resulting summation creates a narrower field of excitation (**Figure 2.2 C-D**). Current focusing is measured in terms of σ, which is the absolute value summation of the percentage of current on the side electrodes [10, 13].

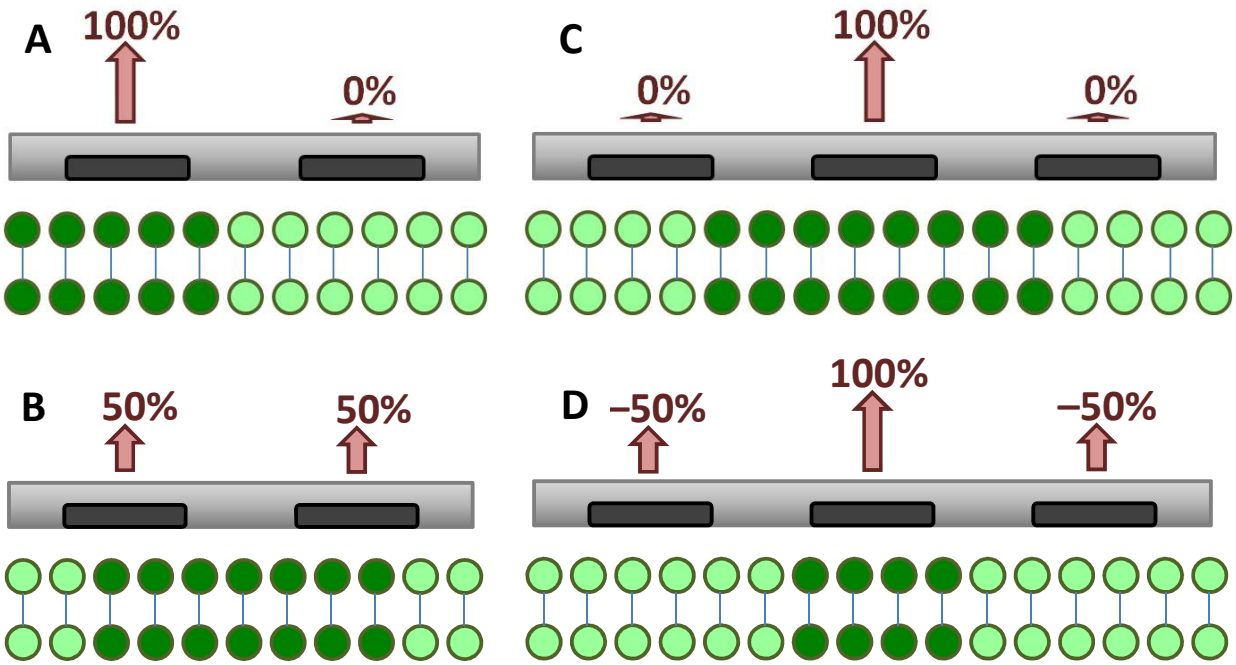

Figure 2.2 – For current steering, **(A)** α = 0 when electrode 1 is stimulated by 100% of the current and electrode 2 is not stimulated, and **(B)** α = 0.5 when electrode 1 is stimulated by 50% and electrode 2 is stimulated by 50%. For current focusing, the center electrode is stimulated by 100% of the current, and **(C)** σ = 0 when the side electrodes are not stimulated, and **(D)** σ = 1 when the side electrodes are stimulated by –50%. Stimulated neurons are darkened.

CHAPTER 3

MODELING EXTRACELLULAR STIMULATION

To simulate and compare high density and contemporary electrodes for cochlear implants, a first order estimation model was developed. The activating function represents the neural response to electrical stimulus and has been incorporated into a neural probability model, which determines the number of neurons fired. A second order estimation model was constructed in COMSOL, a Finite Element Method (FEM) modeling software. For the cochlea and auditory model, the electrode array is located along the *x*-axis, and the auditory neurons are oriented along the *z*-axis. Each auditory neuron contains a cluster of 100 auditory nerve fibers. A distance of *d*, in the *y* direction, separates the electrodes and the fibers (**Figure 3.1**). The equations are evaluated in terms of *x* to view the effects of electrical stimulation across the different neurons.

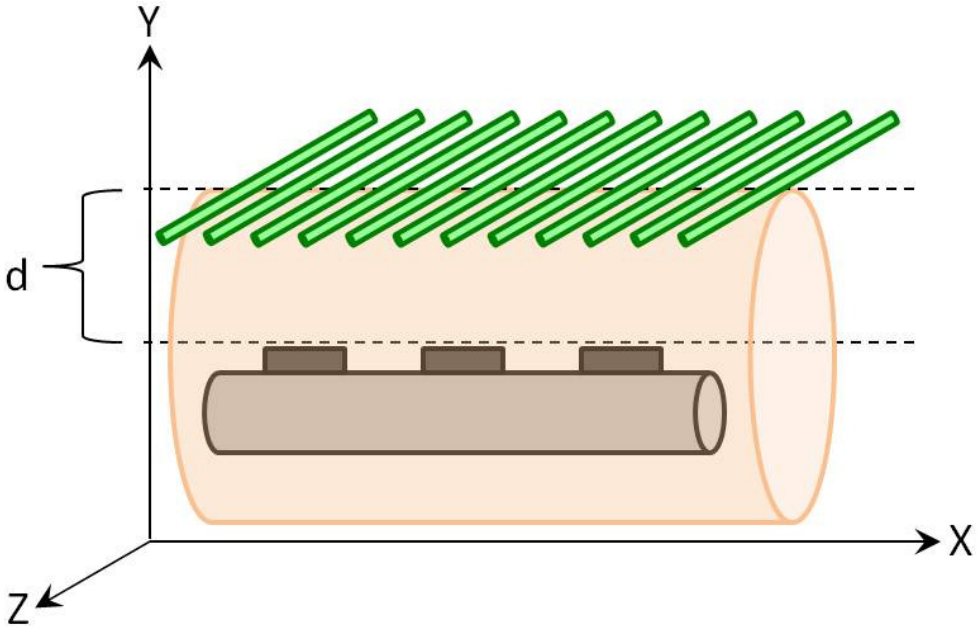

Figure 3.1 – Simplified model of the cochlea (pink), auditory neurons (green), and electrode array (light gray) with electrodes (dark gray).

3.1 Activating Function

The activating function represents the neural response to electrical stimulation. The activating function (**Equation 3.1**) is the second derivative of the neural external potential (**Equation 3.2**). As seen in both equations, ρ_e is the extracellular resistivity, I_{el} is the electrode current, and *x*, *y*, and *z* are the coordinates of the electrode relative to the neuron. The derivative is taken in terms of the coordinate axis that runs parallel to the length of the neuron [14, 15]. For the simplified cochlea and auditory nerve model, the activating function is derived in terms of *z* (the orientation of the neurons). Next, *y* is set equal to *d* and *z* is set equal to 0, leaving *x* and *I* as the inputs for activating function (**Equation 3.3**). For this first order estimate model, the electrodes are represented as point sources [17].

$$AF(x,y,z,I) = \frac{\partial^2 V_e}{\partial z^2} = \frac{\rho_e * I}{4\pi} * \left[\frac{-1}{(x^2+y^2+z^2)^{3/2}} + \frac{\frac{3}{2}z}{(x^2+y^2+z^2)^{5/2}}\right] \quad \textbf{Equation 3.1}$$

$$V_e(x,y,z,I) = \frac{\rho_e}{4\pi} * \frac{I}{\sqrt{x^2+y^2+z^2}} \quad \textbf{Equation 3.2}$$

$$AF(x,I) = \frac{\rho_e * I}{4\pi} * \left[\frac{-1}{(x^2+d^2)^{3/2}}\right] \quad \textbf{Equation 3.3}$$

3.1.1 Derivation

Rattay derived the activating function by manipulating the Hodgkin-Huxley equation (**Equation 3.4**), as follows. **Equation 3.5** defines the relationship between membrane potential (V_n), internal potential (V_i), external potential (V_e) and resting potential (V_r). V_r is set equal to 0 and the resulting equation substitutes V_i in the Hodgkin-Huxley equation, as seen in **Equation 3.6** [14].

$$C_m \frac{d(V_{i,n} - V_{e,n})}{dt} + I_{i,n} + G_a\left(V_{i,n} - V_{i,n-1}\right) + G_a\left(V_{i,n} - V_{i,n+1}\right) = 0 \quad \textbf{Equation 3.4}$$

$$V_n = V_{i,n} - V_{e,n} + V_r \quad \textbf{Equation 3.5}$$

$$\frac{dV_n}{dt} = \frac{1}{C_m}\left[G_a\left(V_{n-1} - 2V_n + V_{n+1} + V_{e,n-1} - 2V_{e,n} + V_{e,n+1}\right) - I_{i,n}\right. \quad \textbf{Equation 3.6}$$

Next, the axon conductance (G_a) is defined in **Equation 3.7** as the inverse of axon resistance (r_s) times the internodal distance (Δx).The ionic current (I_i) is the summation of the sodium current per unit area (i_{Na}), the potassium current per unit area (i_K), and the leakage current per unit area (i_L) (**Equation 3.8**). G_a and I_i are then plugged into the Hodgkin-Huxley equation (**Equation 3.9**) [14].

$$G_a = \frac{1}{r_s \Delta x} \quad \textbf{Equation 3.7}$$

$$I_i = i_{Na} + i_K + i_L \quad \textbf{Equation 3.8}$$

$$\frac{dV_n}{dt} = \frac{1}{C_m}\left[\frac{1}{r_s \Delta x}\left(V_{n-1} - 2V_n + V_{n+1} + V_{e,n-1} - 2V_{e,n} + V_{e,n+1}\right) - \pi d \Delta x (i_{Na} + i_K + i_L)\right] \quad \textbf{Equation 3.9}$$

Last, the membrane capacitance (C_m) is converted into the membrane capacitance per unit area (c_m), as seen in **Equation 3.10**, and plugged in the Hodgkin-Huxley equation (**Equation 3.11**). From this manipulation of the Hodgkin-Huxley equation, the following term can be removed (**Equation 3.12**). By taking the limit of $\tilde{S}(x, t)$ (**Equation 3.13**), the result is the second derivate of the external potential [14].

$$C_m = \pi d \Delta x * c_m \quad \textbf{Equation 3.10}$$

$$\frac{dV_n}{dt} = \frac{1}{c_m}\left[\frac{1}{r_s * \pi d}\left(\frac{V_{n-1} - 2V_n + V_{n+1}}{\Delta x^2} + \frac{V_{e,n-1} - 2V_{e,n} + V_{e,n+1}}{\Delta x^2}\right) - (i_{Na} + i_K + i_L)\right] \quad \textbf{Equation 3.11}$$

$$\tilde{S}(x, t) = \frac{V_{e,n-1} - 2V_{e,n} + V_{e,n+1}}{\Delta x^2} \quad \textbf{Equation 3.12}$$

$$\lim_{\Delta x \to 0} \frac{V_{e,n-1} - 2V_{e,n} + V_{e,n+1}}{\Delta x^2} = \frac{d^2 V_e}{dx^2} \quad \textbf{Equation 3.13}$$

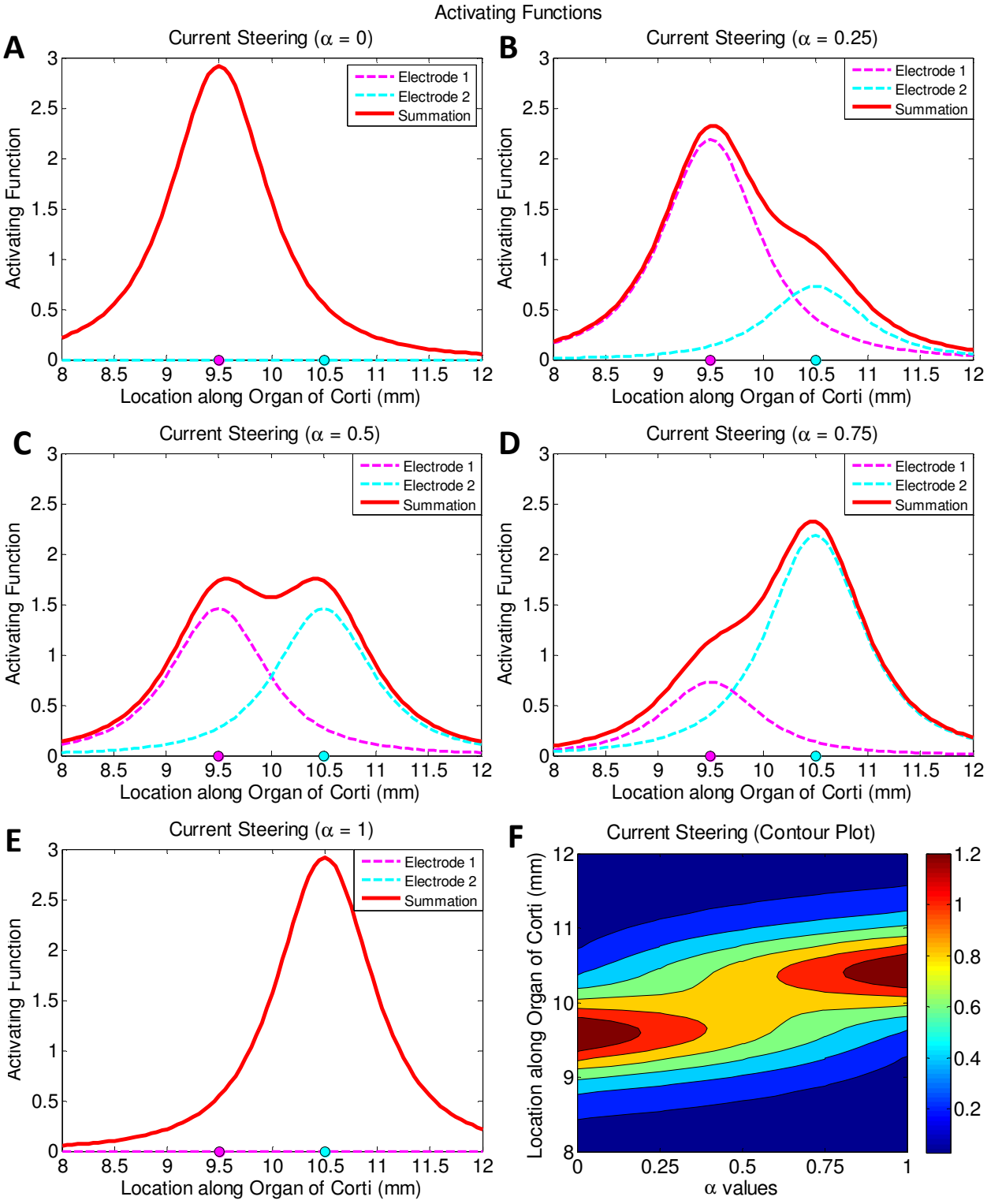

Figure 3.2 – Current steering: **(A)** α = 0 has 100% of the current on the first electrode and 0% of the current on the second electrode, **(B)** α = 0.25 has 75% of the current on the first electrode and 25% of the current on the second electrode, **(C)** α = 0.5 has 50% of the current on the first electrode and 50% of the current on the second electrode, **(D)** α = 0.75 has 25% of the current on the first electrode and 75% of the current on the second electrode, and **(E)** α = 1 has 0% of the current on the first electrode and 0% of the current on the second electrode. **(F)** is the contour plot of the collective current steering plots (x-axis is the α values, y-axis is the location along the cochlea, and the color bar is the activating function).

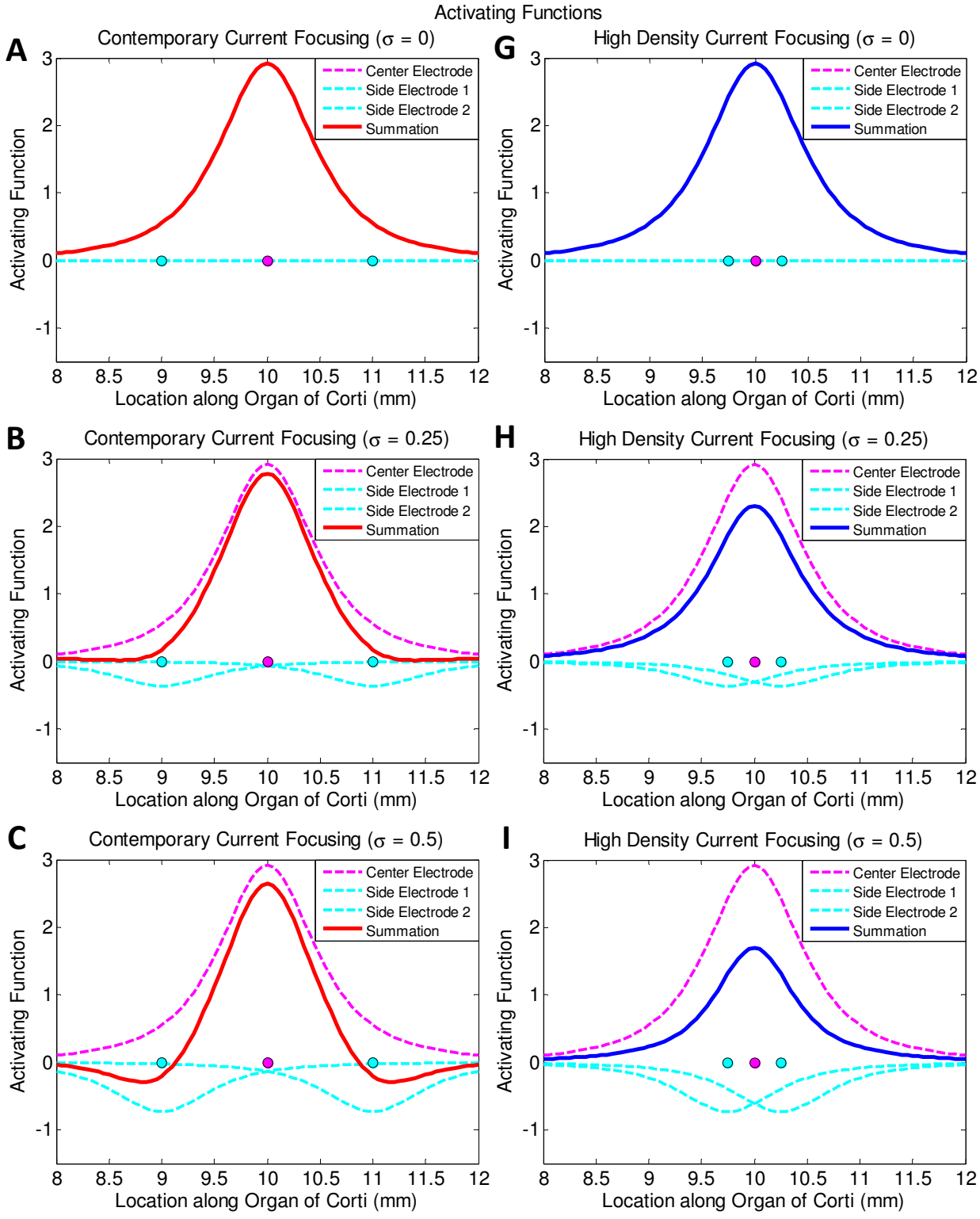
Activating Functions
A
Contemporary Current Focusing (σ = 0)
G
High Density Current Focusing (σ = 0)
B
Contemporary Current Focusing (σ = 0.25)
H
High Density Current Focusing (σ = 0.25)
C
Contemporary Current Focusing (σ = 0.5)
I
High Density Current Focusing (σ = 0.5)
Center Electrode
Side Electrode 1
Side Electrode 2
Summation
Activating Function
Location along Organ of Corti (mm)
3
2
1
0
-1
8
8.5
9
9.5
10
10.5
11
11.5
12

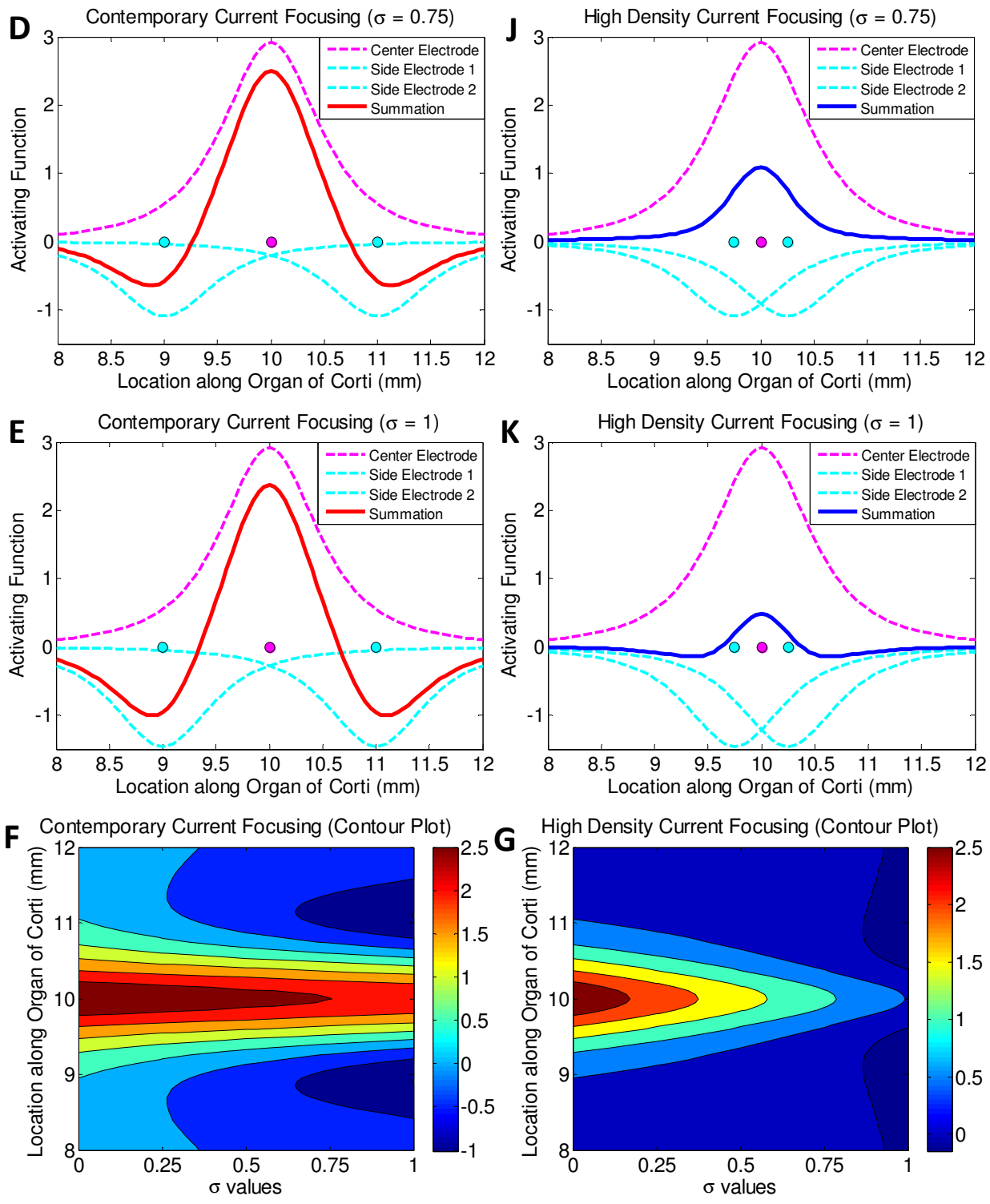

Figure 3.3 – **(A-F)** are contemporary current focusing and **(G-L)** are high density current focusing: **(A,G)** σ = 0 has 100% of the current on the center electrode and a total of -0% of the current on the side electrodes, **(B,H)** σ = 0. 25 has 100% of the current on the center electrode and a total of -25% of the current on the side electrodes, **(C,I)** σ = 0.5 has 100% of the current on the center electrode and a total of -50% of the current on the side electrodes, **(D,J)** σ = 0.75 has 100% of the current on the center electrode and a total of -75% of the current on the side electrodes, and **(E,K)** σ = 1 has 100% of the current on the center electrode and a total of -100% of the current on the side electrodes. **(F,L)** are contour plots of the collective current focusing plots (x-axis is the σ values, y-axis is the location along the cochlea, and the color bar is the activating function).

3.1.2 Current Steering and Current Focusing

The activating function for current steering is the summation of the activating functions of the first electrode (located at x_1) and the second electrode (located at x_2). According to the current steering definition, the input current (I) of the first electrode is multiplied by ($1 - \alpha$) and I of the second electrode is multiplied by α (**Equation 3.14**) [16]. **Figure 3.2** illustrates current steering between two electrodes with values of α ranging from 0 to 1. The activating function for current focusing is the summation of the activating functions of the first electrode (located at x_1), the second electrode (located at x_2), and the third electrode (located at x_3). According to the current focusing definition, I of the first and third electrode is multiplied by $-\sigma/2$, and I of the second electrode is not altered (**Equation 3.15**) [17]. **Figure 3.3** illustrates current focusing for both three contemporary electrodes and three high density electrodes with values of σ ranging from 0 to 1. All plots were calculated with $I = 1mA$.

$$AF_{CS} = AF_1(x_1, (1-\alpha) * I) + AF_2(x_2, \alpha * I) \quad \textbf{Equation 3.14}$$

$$AF_{CF} = AF_1(x_1, -\sigma/2 * I) + AF_2(x_2, I) + AF_3(x_3, -\sigma/2 * I) \quad \textbf{Equation 3.15}$$

3.2 Greenwood Function

The Greenwood function was derived to map the frequency-to-position relation of the cochlea (**Equation 3.16**). The frequency (f) is calculated in terms of distance along the cochlea (x). The apex of the cochlea is at $x = 0$. The remaining terms are constants. A is a frequency scaling constant set to 165.4, K is a frequency integration constant set to 0.88, and a is a frequency-position slope set to 0.06 if x is in mm and 2.1 if x is a fraction of the distance of the cochlea [18]. The equation was modified to set the base of the cochlea to $x = 0$. The total length of the cochlea was set to 31 mm, as recorded by Stakhovskaya (**Equation 3.17**) [19]. Using the Greenwood function, the x variable in the activating function and the following neural firing probability model was converted into frequency [20].

$$f(x) = A(10^{ax} - K) \quad \textbf{Equation 3.16}$$

$$f(x) = A(10^{a(31-x)} - K) \quad \textbf{Equation 3.17}$$

3.3 Neural Firing Probability Model

The following model calculates the firing probability of a single nerve fiber (*j*) due to electrical stimulation (**Equation 3.18**). The probability is calculated by subtracting the activating function threshold (AF_{thr}) from the absolute value of the activating function. The difference is divided by the multiple of the activating function threshold and the relative spread (*RS*). Finally, the cumulative normal distribution (Φ) is taken and the probability is determined. The relative spread is a constant that relates firing probability to stimulus threshold. It is calculated by generating a random number from a normal distribution with a mean of 0.0635 and a standard deviation of 0.04. The resulting number is then clipped within the range of 0.03 and 0.1. The activating function threshold is determined by generating a random number from a log-normal distribution, which is assumed to have a standard deviation to mean ratio of 0.3. The mean of the activating function threshold is arbitrarily set to 0 dB. This arbitrary assignment is inconsequential when comparing the relative neural activity levels [17].

$$P(x,j) = \Phi\left[\frac{|AF(x,I_{el})| - AF_{thr}(x,j)}{AF_{thr}(x,j) * RS(x,j)}\right] \qquad \textbf{Equation 3.18}$$

To calculate the neuron's binary firing response, a uniformly distributed random variable (*RV*) is generated between 0 and 1. The probability is compared to *RV*. If the probability is greater than or equal to *RV*, the neuron discharges (*N*) as seen in **Equation 3.19**. For each neural cluster at *x*, all fired neurons are summed (ΣN) [21]. The assumption was made that ΣN equaled the loudness heard by the cochlear implant patient. Therefore, the different stimulation scenarios were compared relatively via summed total number of neurons fired (ΣN) [16]. The following ΣNs were analyzed: 250, 500, 1000, and 2000.

$$N(x,j) = \begin{cases} 1 \; if \; P(x,j) \geq RV \\ 0 \; if \; P(x,j) < RV \end{cases} \qquad \textbf{Equation 3.19}$$

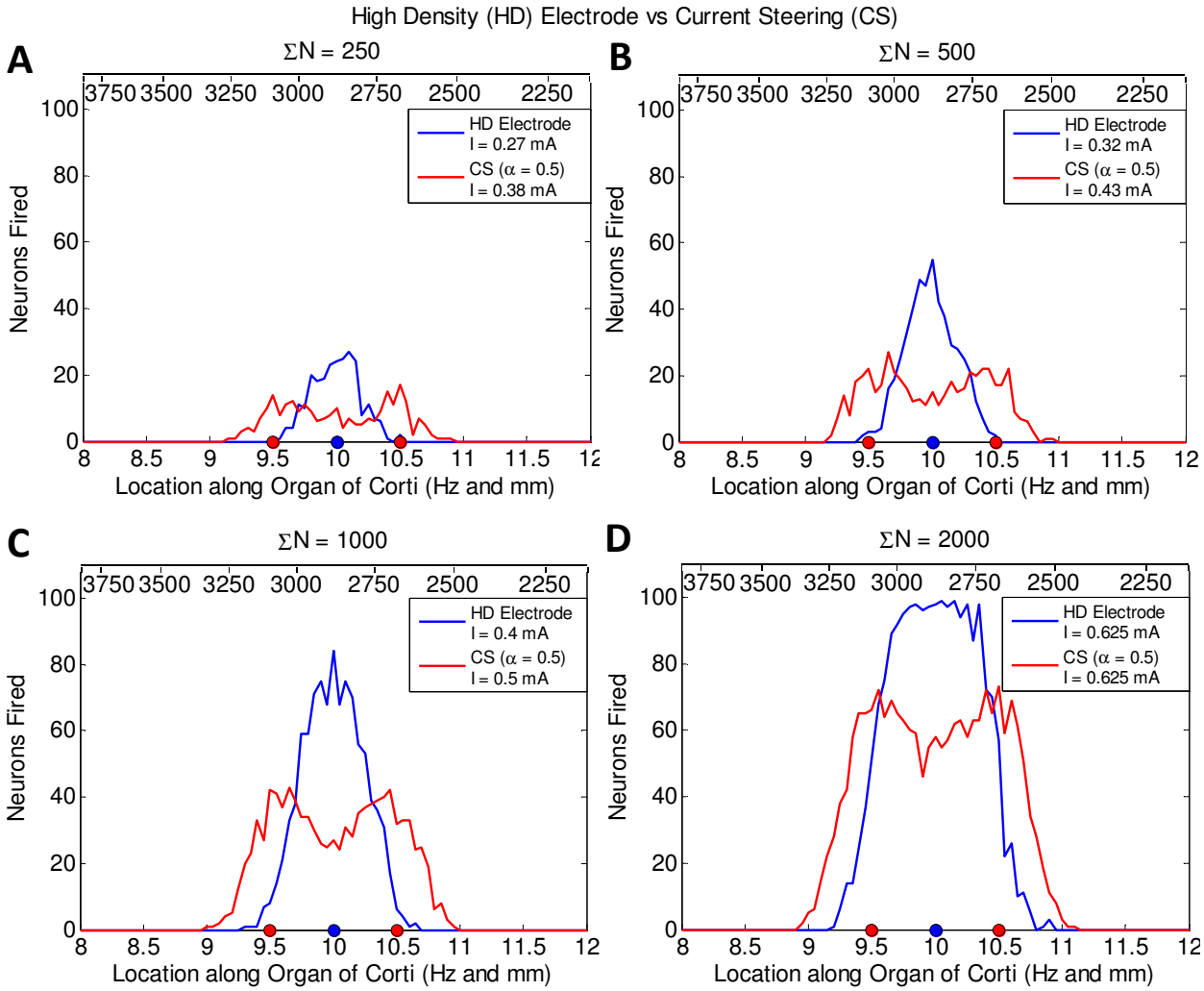

Figure 3.4 – Comparison of a high density (HD) electrode to current steering (CS): **(A)** for *ΣN = 250*, *I = 0.27 mA* for HD Electrode and *I = 0.38 mA* for CS, **(B)** for *ΣN = 500*, *I = 0.32 mA* for HD electrode and *I = 0.43 mA* for CS, **(C)** for *ΣN = 1000*, *I = 0.4 mA* for HD electrode and *I = 0.5* for CS, **(D)** for *ΣN = 2000*, *I = 0.625 mA* for HD electrode and *I = 0.625 mA* for CS. The y-axis is the number of neurons fired. The top x-axis is the calculated Greenwood frequency (Hz) and the bottom x-axis is the location along the Organ of Corti in the cochlea (mm).

3.3.1 Results

Two different stimulation scenarios were evaluated: current steering vs. a high density electrode and current focusing of contemporary electrodes vs. current focusing of high density electrodes. For the first scenario, there were two contemporary electrodes, located at 9.5 mm and 10.5 mm for a 1 mm separation distance. These two electrodes underwent current steering with α = 0.5, which should stimulate the neural population around 10 mm (equidistance between the two electrodes) [20]. This neural response was then compared to that of a high density electrode located at 10 mm. As shown in

Figure 3.4, current steering and the high density electrode were normalized by the summed total neurons fired (*ΣN = 250, ΣN = 500, ΣN = 1000, ΣN = 2000*). With each *ΣN*, the high density electrode produced a more localized stimulation then its current steering counterpart. The high density electrode consumed less current until reaching *ΣN = 2000*, where the current consumption was equal for both the high density electrode and current steering.

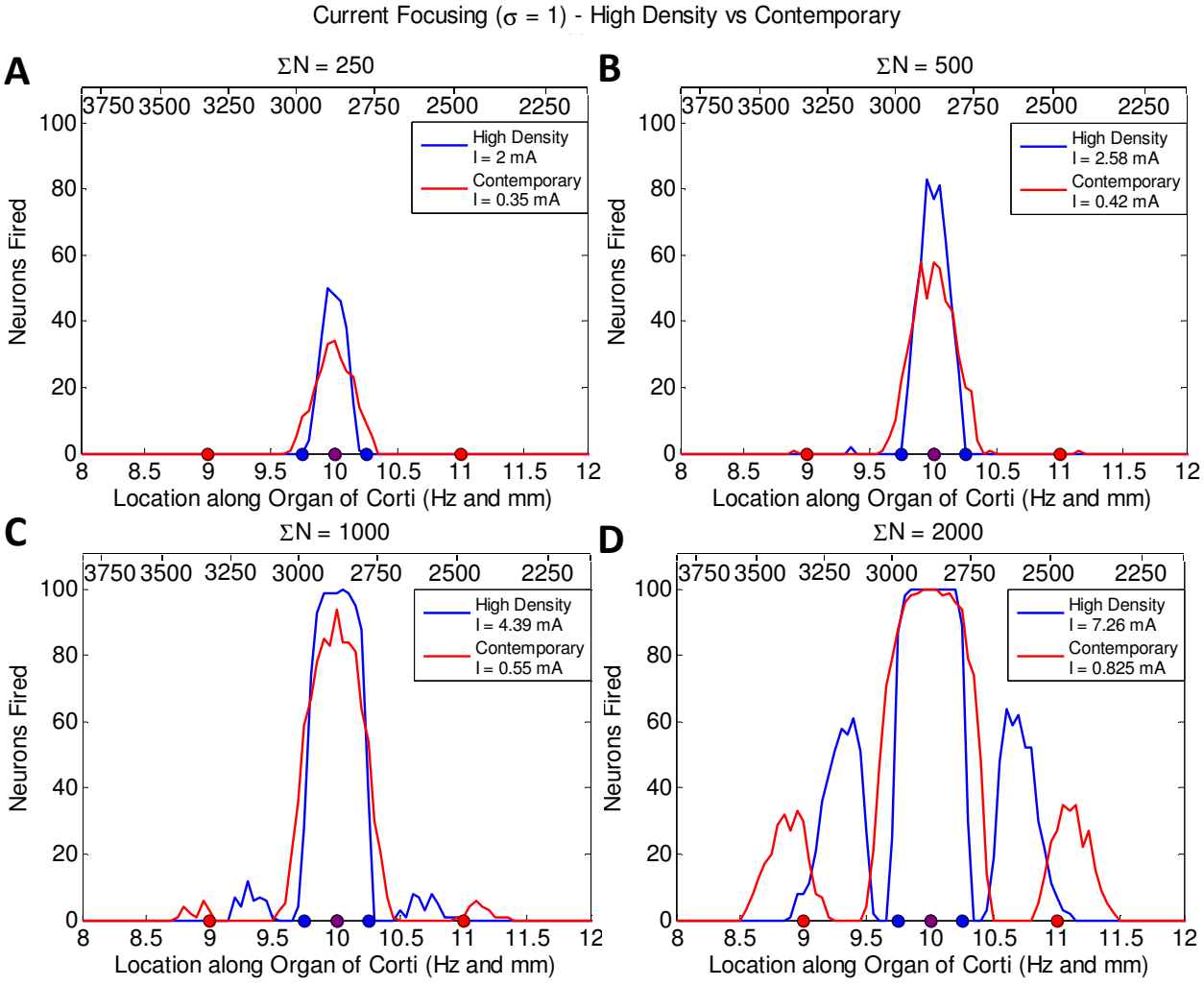

Figure 3.5 – Comparison of current focusing with *σ = 1* for high density electrodes and contemporary electrodes: **(A)** for *ΣN = 250*, *I = 2 mA* for high density and *I = 0.35 mA* for contemporary, **(B)** for *ΣN = 500*, *I = 2.58 mA* for high density and *I = 0.42 mA* for contemporary, **(C)** for *ΣN = 1000*, *I = 4.39 mA* for high density and *I = 0.55* for contemporary, **(D)** for *ΣN = 2000*, *I = 7.26 mA* for high density and *I = 0.825 mA* for contemporary. The y-axis is the number of neurons fired. The top x-axis is the calculated Greenwood frequency (Hz) and the bottom x-axis is the location along the Organ of Corti in the cochlea (mm).

For the second scenario, current focusing with *σ = 1* was compared between three contemporary and three high density electrodes. The contemporary electrodes were located at 9 mm,

10 mm, and 11 mm, with an end-to-end spacing of 1 mm. The high density electrodes were located at 9.75 mm, 10 mm, and 10.25, with an end-to-end spacing of 0.25 mm, as found in [3]. As seen in **Figure 3.5**, the contemporary and high density electrodes were normalized by the summed total neurons fired ($\Sigma N = 250$, $\Sigma N = 500$, $\Sigma N = 1000$, $\Sigma N = 2000$). Current focusing using high density electrodes appeared to create a more focused neural response; however, current consumption of current focusing with high density electrodes was a whole order of magnitude higher than current focusing with contemporary electrodes.

3.3.2 Discussion

When comparing current steering to high density electrodes, the neural probability model shows that high density electrodes are more localized. While current steering does activate previously unstimulated fibers, placing a high density electrode beneath the same fibers creates a more precise spread of excitation. **Figure 3.2 C** demonstrates why current steering produces a wider spread of excitation and stimulates fewer neurons than a high density electrode. For current steering, the activating functions for two electrodes are summed, and the resulting activating function is almost twice as wide as the activating function from a single electrode. Also, note that while the activating functions from the two electrodes overlap to stimulate centrally located neurons, due to the electrode spacing, the spread of excitation is weakest in the center of the current steering activating function. As a result, current steering requires greater current to stimulate the same number of neurons as a single high density electrode.

With current focusing, the only difference observed between contemporary and high density electrodes was at $\sigma = 1$. While the spread of excitation generated by the high density electrodes was narrower, the current required to activate the same number of neurons as the contemporary electrodes was an order of magnitude higher for the high density electrodes. The reason for this scenario is illustrated in **Figure 3.3 E** and **Figure 3.3 J**. The activating functions of the current focusing ($\sigma=1$) for

contemporary and high density electrodes are displayed. Note that for the contemporary electrodes, since the spacing is 1 mm, the side electrodes do not greatly detract from the strength of the final summation. However, for the high density electrodes, the spacing of 0.25 mm is a disadvantage, as the side electrodes have a much greater impact on the strength of the final summation. Therefore, the current on the high density electrodes must be exponentially increased to maintain the effectiveness of the contemporary electrodes.

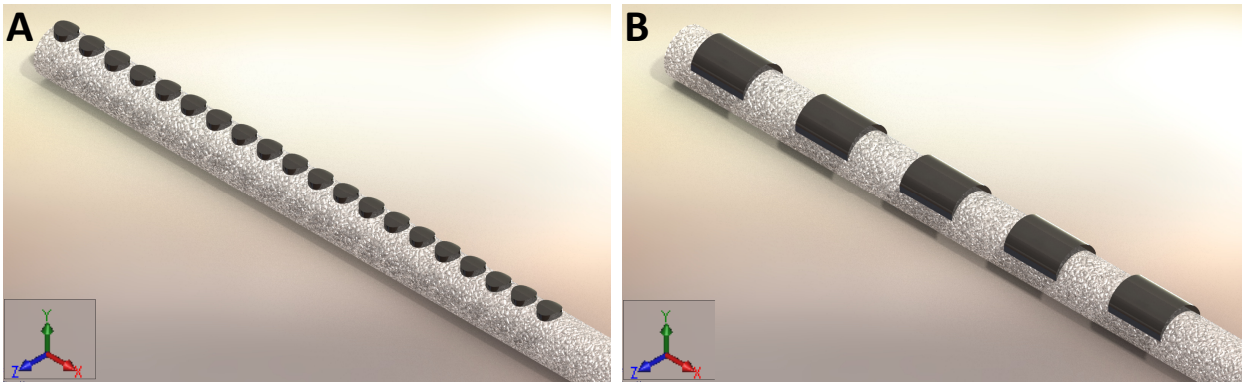

Figure 3.6 – 3D CAD models of **(A)** a high density cochlear implant (electrode diameter = 180 µm and electrode midpoint spacing = 250µm) and **(B)** a generic, contemporary cochlear implant (electrode diameter = 0.5 mm and electrode midpoint spacing = 1 mm)

3.4 Finite Element Method

COMSOL (Burlington, MA) is a finite element method (FEM) modeling software used for physics-based device simulations. Three dimensional, computer-aided design (CAD) models of both a high density and contemporary cochlear implant (**Figure 3.6**) were designed in SolidWorks (Concord, MA). The electrodes of the high density cochlear implant have a diameter of 180 microns and a midpoint spacing of 250 microns [3, 22]. The electrodes of the generic, contemporary cochlear implant have a diameter of 0.5 mm and a midpoint spacing of 1 mm. For both implants, an external ground electrode was placed on the extended array 5mm away from the main electrodes. The CAD models were imported into the Conductive Media DC module of COMSOL. The cochlea was represented by a cylinder with a diameter of 1.2 mm (the height of the human cochlea ~7mm from the round window) and a conductivity of 1 S/m [22]. Both electrode arrays were oriented inside the cochlea along the x-axis. The

center of the array was located at z = 0, and in the y direction, the tops of the electrodes were 0.7 mm away from the edge of the cochlea [17].

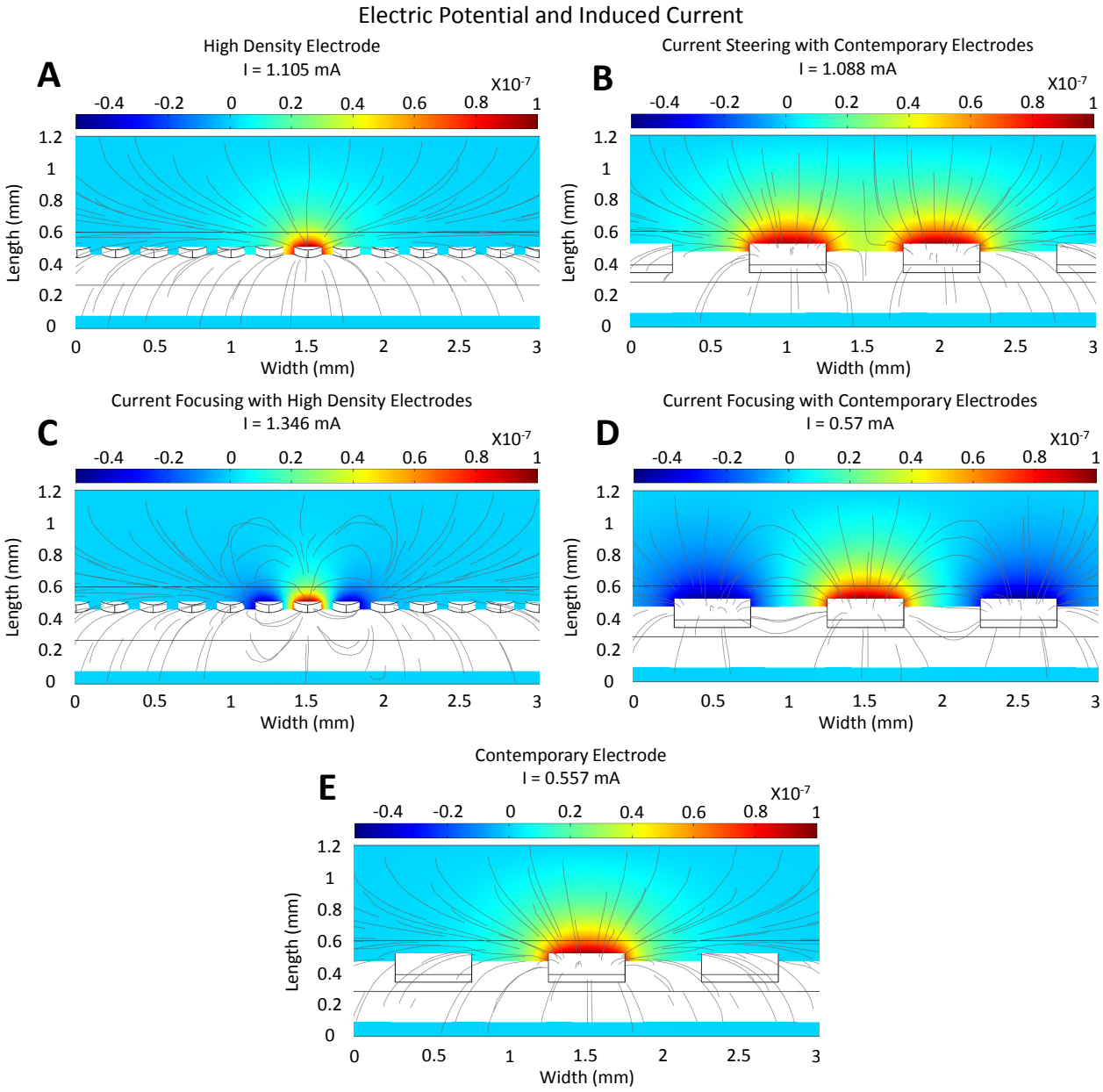

Figure 3.7 – Electric potential (colored bar) and induced current (gray lines) for **(A)** a high density electrode (I = 1.105 mA generates a max potential of $1x10^{-7}$ V), **(B)** current steering with contemporary electrodes (I = 1.088 mA generates a max potential of $1x10^{-7}$ V), **(C)** current focusing with high density electrodes (I = 1.346 mA generates a max potential of $1x10^{-7}$ V), **(D)** current focusing with contemporary electrodes (I = 0.57 mA generates a max potential of $1x10^{-7}$ V), and **(E)** a contemporary electrode (I = 0.557 mA generates a max potential of $1x10^{-7}$ V)

3.4.1 Results

The generated electric potential (colored bar) and induced current (gray lines) are shown for a single high density electrode (**Figure 3.7 A**), current steering with two contemporary electrodes (**Figure 3.7 B**), current focusing with three high density electrodes (**Figure 3.7 C**), current focusing with three contemporary electrodes (**Figure 3.7 D**), and a single contemporary electrode (**Figure 3.7 E**). The generated electric potentials were normalized to a maximum potential of $1x10^{-7}$ V (dark red) and a minimum potential of $-0.5x10^{-7}$ V (dark blue). The applied current required to generate $1x10^{-7}$ V at the surface of the electrode is also shown in the title of each plot.

3.4.2 Discussion

The COMSOL plots in **Figure 3.7** provide a basic representation of the effects of electrical stimulation in a conductive media, such as the cochlea. However, further work is needed to properly interpret the results in terms of neural stimulation. The generated potentials and current from COMSOL can be used in a neural simulator, such as NEURON (Yale, VA) [23]. In NEURON, physiologically accurate models of the auditory nerve fibers would be created. By combining dimensionally accurate electrode arrays and anatomically accurate auditory nerve fibers, the generated results will more accurately demonstrate the effects of high density electrode stimulation on the auditory nerve fibers.

CHAPTER 4

DEVICE INTEGRATION

Contemporary electrode arrays are composed of a wire encased in silicone. These structures are easily bent to accommodate the curved and tapered cochlea. TFMs are planar, ribbon-shaped devices, which provide some restraints with flexibility. To solve this issue, an insertion platform (IP) was used. Section 4.1 outlines troubleshooting and provides the final assembly protocol. Section 4.2 reviews the structural tests conducted in cadaver cochleae.

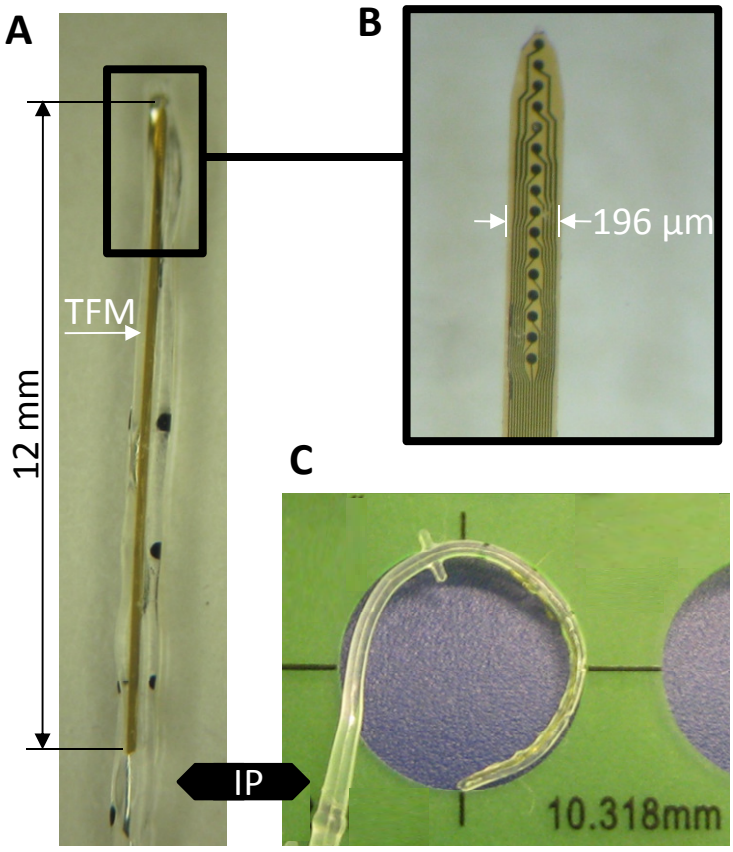

Figure 4.1 – (A) Fully assembled TFM (gold) and IP (clear). **(B)** Magnified view of the TFM. **(C)** TFM/IP test in circle stencil.

4.1 Assembly

In order to pursue physiologically testing, a successful assembly protocol to adhere the TFM array to the IP was needed. The manufactured TFM array (NeuroNexus Technologies; Ann Arbor, MI) was composed of polyimide with 16 platinum, electrode sites. The TFM array had a length of 12 mm and a width of 196 µm (**Figure 4.1 A** and **B**). For the IP, an electrically inactive, Med-El insertion test device (Med-El; Innsbruck, Austria) was used. The insertion test device had a distal width of 0.5 mm and an insertion length of 17 mm, as measured from the distal end to the t-stopper. The t-stopper is visible in **Figure 4.1 C**. To adhere the two devices, a silicone adhesive (Med-2000, Nusil Silicone Technologies; Carpinteria, CA) was used. Procedures for the following tasks were determined: 1) application of the adhesive, 2) mounting the TFM array, and 3) promotion of bonding between the TFM array and the adhesive.

Table 4.1 – Concise overview of assembly protocol for TFM/IP

Step	Action	Tools
1	Stabilize IP	IP, water-soluble wax, glass slide, hot plate
2	Apply Adhesive	Adhesive, digital controlled dispenser
3	Mount TFM Array	TFM array, vacuum pick
4	Promote Bonding	Tweezers
5	Dry	
6	Release	Water

4.1.2 Protocol

- Step 1: Water-soluble wax is melted onto a glass slide. While the wax is still hot, the IP is straightened and placed into the wax. The IP is held in place while the wax cools.
- Step 2: The digital controlled dispenser is assembled. A 25 gauge dispensing tip is attached to the application cartridge, and the silicone adhesive is inserted into the cartridge. The dispenser is set to Pressure = 440 lbs/in, Interval = 1 sec, and Dispensing Time = 1.1 sec. Using the microscope, a straight, ~12 mm line of adhesive is applied, originating from the tip of the IP.

- Step 3: Using the vacuum pick with a 25 gauge probe tip that has been bent to ~80° angle, a TFM array is selected. The probe of the vacuum pick is secured in microelectrode holder. Using the microscope, the TFM is oriented and deposited on the glue.
- Step 4: Using tweezers, the TFM is gently pressed into the glue.
- Step 5: Leave the TFM/IP to dry for 24 hours.
- Step 6: Next, the glass slide is run under warm water to remove the wax and the TFM/IP is released.

A preliminary test can be conducted to immediately identify if the bond is secure. The TFM/IP is inserted 270° into a ~10mm diameter circle cutout (the distance and angle are equal to a typical cochlear implant insertion) as seen in **Figure 4.1 C**. The TFM array will immediately delaminate from the IP if the bond was unsuccessful. **Table 4.1** provides a brief overview of the actions performed and the tools needed for each step.

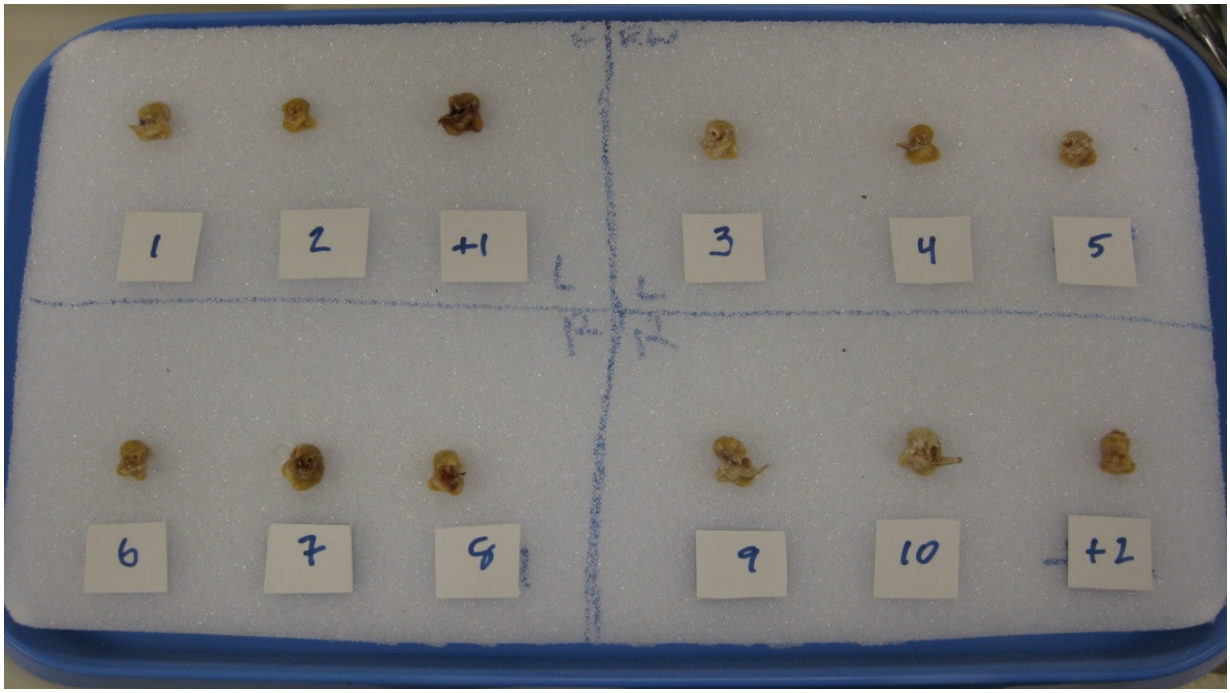

Figure 4.2 – The 12 harvested cochleae for implantation (Row 1 are left ear cochleae and row 2 are right ear cochleae. Columns 1 – 3 are cochleostomy and columns 4 – 6 are round window. The positive controls are labeled).

4.2 Structural Tests with Cadaver Cochleae

As mentioned previously, the planar structure of the TFM array could be problematic with insertion. The overarching goals of these experiments are to conduct animal studies, and eventually graduate to clinical trials. However, these objectives will not be realized if a basic insertion cannot be achieved with the TFM/IP assembly. In collaboration with Medical College of Georgia, the in vitro cochleae tests were performed. The Medical College of Georgia team harvested 14 human cadaver cochleae (**Figure 4.2**), and a cochleostomy implantation of the TFM/IP was performed on 6 cochleae and a round window implantation of the TFM/IP was performed on the other 6 cochleae (**Figure 4.3 A**). There were 2 positive control cochleae, which were implanted with an unaltered IP, and 2 negative control cochleae, which were not implanted. Both positive and negative controls had 1 cochleostomy and 1 round window. All insertions were performed by Dr. Ken Iverson and were recorded using real-time fluoroscopy (**Figure 4.3 B**). Post-insertion computer tomography (CT) scans (**Figure 4.3 C**) and histological evaluations were conducted by the Medical College of Georgia team [24].

The Medical College of Georgia team prepared the cochleae by serially dehydrating the specimens in increasing concentrations of ethanol (50%, 70%, 80%, 95%, and 100%). The specimens were washed in xylene for 24 hours. For plasticization of the cochleae, the specimens were placed in increasing concentrations of methyl methacrylate in a warming oven. Next, using a diamond saw blade, the cochleae were sectioned along the modiolus for a cross section of the scala tympani and vestibuli. Following Wardrop et al's protocol, severity trauma was evaluated in osseous spiral lamina, basilar membrane, spiral ligament, and Reissner's membrane, and an overall percentage of trauma was calculated for each cochlea [24].

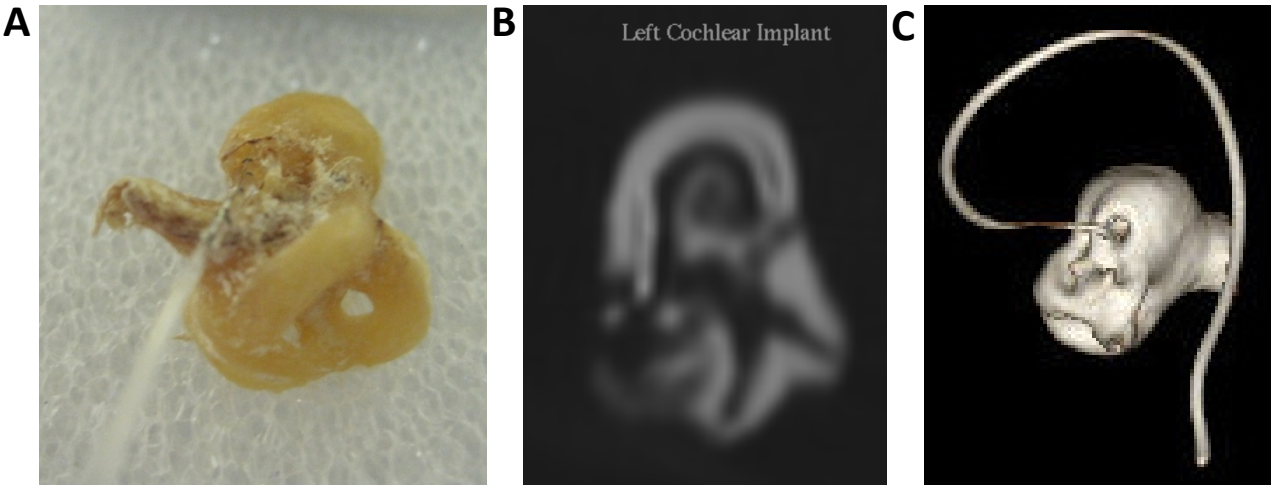

Figure 4.3 – (A) Cochlea post-implantation of the TFM/IP. **(B)** Fluoroscopy image of TFM/IP implanted cochlea. **(C)** CT scan 3D reconstruction of TFM/IP implanted cochlea.

4.2.1 Results

All 10 TFM/IP arrays were fully inserted into the cochleae. Of the 10 implanted TFM/IPs, only 2 required readjustments. 1 TFM/IP required 2 readjustments, and another TFM/IP visibly delaminated upon initial insertion and required 3 readjustments. As measured from the fluoroscopic images, the mean angular depths for the TFM/IP implantations were 292°. The positive controls were 325°. Proximal kinking was recorded in 3 of the implantations in the basal turn. An example of proximal kinking is provided in **Figure 4.4 C** [24].

In the histological evaluation, a total 3 TFM arrays delaminated and folded onto themselves. The insertion trauma was analyzed along the unwinded length of the cochlea for each specimen. The trauma for all electrode insertions was 23.5%. The positive control had 12.8% trauma and the negative control had 28.8% trauma. 1 TFM/IP was malinserted into the scala vestibuli (**Figure 4.4 B**), and 3 TFM/IPs demonstrated scala vestibuli excursion (**Figure 4.4 D, E**). The average angular depth for all TFM/IP insertions was 391.5° and for the positive controls was 405°. The TFM/IP arrays rotated towards the apex with a mean of 87.4°, making the average distance from the electrodes to the modiolus 1.4 mm. The closest point to the modiolus for the TFM/IPs was 0.67 mm and for the positive controls was 0.86 mm [24].

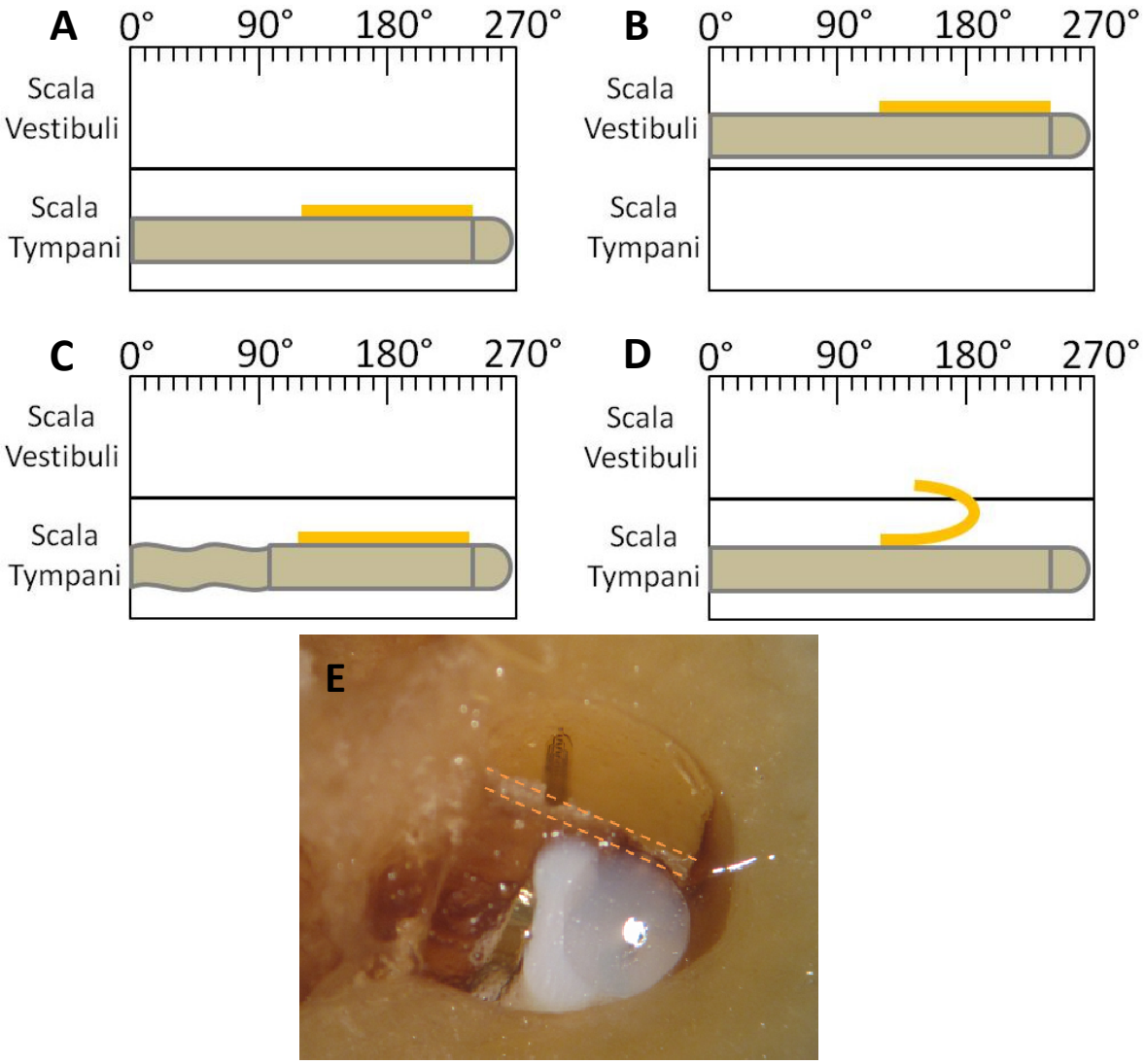

Figure 4.4 – 2D drawings of unrolled cochleae with the location of the TFM/IP for **(A)** normal insertion, **(B)** scala vestibuli insertion, **(C)** proximal kinking, and **(D)** scala vestibuli excursion of the TFM array. The gray cylindrical shape is the IP and the gold rectangle is the TFM array. **(E)** Histological cross section of scala vestibuli excursion of TFM array, where the white circle is the IP (located in the scala tympani), the gold ribbon is the TFM array (partially located in the scala tympani and vestibuli), and the tan dashed lines outlines the basilar and Reissner's membrane.

4.2.2 Discussion

Table 4.2 presents a comparison of the implanted TFM/IP arrays to the positive control IPs and previously collected data by Wardrop et al for Cochlear Ltd and Advanced Bionics' cochlear implants. Wardrop et al's angular and linear depths were measured from 2D x-ray images that were analyzed with Canvas™ software. The specimens then underwent histological processing in which the severity of trauma was analyzed and the occurrence of scala vestibuli excursion and insertion were recorded [25,

26]. For the depth inserted (17 mm), the TFM/IPs have a higher percentage of trauma than the IPs and other cochlear implants with a similar linear depth. However, the fact that the negative control (the non-implanted cochleae) had trauma of 28.8% is a reason to investigate the cochlea harvesting technique, and perhaps question the inflation of the recorded trauma values. While the scala vestibuli excursion for the TFM/IPs was due to the delaminated TFM array, the number of occurrences is within a normal range. In a study conducted by Ketten et al., 4 out of 20 Nucleus cochlear implantations were reported to have proximal kinks [27]. It does not appear that the 3 recorded proximal kinks are unique to the TFM/IP array.

Table 4.2 – Comparison of TFM/IP and IP to Cochlear's Banded and Contour cochlear implants and Advanced Bionics' Spiral Clarion and HiFocus II cochlear implants (SI = Shallow Insertion and DI = Deep Insertion).

Company	***Research***		**Cochlear Ltd.**			**Advanced Bionics**		
Cochlear Implant	*TFM/IP*	*IP*	*Nucleus Banded*	*Nucleus Contour*	*Spiral Clarion (SI)*	*Spiral Clarion (DI)*	*HiFocus II (SI)*	*HiFocus II (DI)*
Avg Linear Depth (mm)	17	17	15.3	17.9	16.75	24.95	~17	~23
Avg Angular Depth (°)	291.8	324.5	285	417	304.5	492.3	332.6	508.7
Avg Trauma (%)	23.5	12.8	~16	~13	~9	~32	~8	~46
Scala Vestibuli Excursion	20% (3/10)	0% (0/2)	12.5% (1/8)	39% (7/18)	0% (0/2)	33.3% (2/6)	0% (0/14)	50% (3/6)
Scala Vestibuli Insertion	10% (1/10)	0% (0/2)	25% (2/8)	0% (0/18)	0% (0/2)	0% (0/6)	0% (0/14)	0% (0/6)

An interesting observation is that the all of the scala vestibuli excursions were caused by the TFM arrays that folded over onto themselves. This was probably due to the TFM array delaminating during insertion and subsequently puncturing the basilar and Reissner's membrane. This data indicates that the distal end of the TFM array is most likely to cause damage should it delaminate during the insertion. Reinvestigation of the adhesion technique has been implemented. A silicone primer will be applied to the TFM array to increase bonding. The distal end of the TFM array will also be placed ~0.5

mm from the distal end of the IP to correspond with the first electrode of a contemporary electrode array. This new parameter will allow the distal end of the TFM array to be properly mounted to the IP. Another key issue is the almost 90° rotation the TFM arrays underwent during insertion. Through a discussion with Stefan B. Nielsen, a R&D Engineer at Med-El, it was discovered that the ITDs have been designed to rotate in the plane normal to the t-stopper [28]. The TFM arrays were mounted on the ITD perpendicular to the t-stopper. Therefore, the 90° rotation could be from the ITD and not the TFM array. All future devices will mount the TFM array normal to the t-stopper.

CHAPTER 5

CONCLUSIONS AND FUTURE RESEARCH DIRECTIONS

The purpose of the research was to validate the increased performance of high density electrodes for cochlear implants. Simulations were used to observe the effects of high density electrodes on neural stimulation, and in vitro experiments were used to confirm the structural integrity of the TFM/IP devices. The simulations were composed of a first order estimation model, which fused the activating function with a neural firing probability model, and a second order estimation model, which required COMSOL. The in vitro experiments were conducted by inserting the TFM/IP devices into human cadaver cochleae. From the first order estimation model, high density electrodes were shown to provide a more precise stimulation then current steering, an alternate method offered in contemporary electrodes. The second order estimation model provided a detailed analysis of the potential differentials and current flow generated by the electrodes in a conductive media (aka the cochlea). For the structural tests, the TFM/IP devices did not have a higher occurrence of scala vestibuli excursion when compared to similar data collected from contemporary electrode arrays.

Currently, the arrangement of in vivo animal tests is underway. The data collected from these experiments will provide a more accurate and detailed synopsis of how the high density electrodes interact with the auditory nerve fibers. The assembly for the TFM/IP devices will be improved for the animal tests to promote maximum bonding of the TFM array to the silicone substrate. Future work for the simulations will include adding a neural component to the second order estimation model. This will allow the user to compare 3D accurate models of the electrode arrays and evaluate the effects of the electrodes' dimensions on neural stimulation.

REFERENCES

[1] **"**Cochlear Implants**,"** *National Institute on Deafness and Other Communication Disorders*, http://www.nidcd.nih.gov/health/hearing/coch.asp, March 2011.

[2] B. Wilson and M. Dorman, "Cochlear implants: Current designs and future possibilities," *Journal of Rehabilitation Research and Development*, 45(5): 696-730, 2008.

[3] K. D. Wise, P. T. Bhatti, J. Wang, and C. R. Friedrich, "High-density cochlear implants with position sensing and control," *Hearing Research Journal.* 242:22-30, 2008.

[4] "Mimicking the Human Ear," *IEEE Signal Processing Magazine*, pages 101-130, September 1998.

[5] Advanced Bionics, LLC , "HiFocus Helix® and HiFocus® 1J Electrodes," http://www.advancedbionics.com/For_Professionals/Technical_Product_Details/HiFocus_Helix_and__HiFocus_1J_Electrodes.cfm?langid=1, March 2011.

[6] Advanced Bionics, LLC, "HiFocus Electrode Series," http://www.advancedbionics.com/userfiles/File/HiFocus_Helix_Electrode.pdf/, March 2011.

[7] Cochlear Limited, "Nucleus® 5 Cochlear Implant (CI512) – Technical Specifications," http://professionals.cochlearamericas.com/sites/default/files/resources/Nucleus%205%20Cochlear%20Implant%20Technical%20Specifications%20(CI512)%20FUN1007%20ISS3%20AUG09.pdf, March 2011.

[8] Med-El, "Products - PULSARCI^{100} Technical Specifications," http://www.cochlearimplants.com/ENG/US/20_Products/10_Cochlear_Implants/999_p_tech.asp, March 2011.

[9] Neurelec, " Digisonic® SP," http://www.neurelec.com/images/photos/digisonic_SP_en.pdf, March 2011.

[10] B. Bonham and L. Litvak, "Current focusing and steering: Modeling, physiology, and psychophysics," *Hearing Research*, 242(1-2): 141-153, August 2008.

[11] Advanced Bionics©, "HiRes with Fidelty™ 120 Sound Processing," [White Paper] *Boston Scientific*, Sept 2006.

[12] J. B. Firszt, D. B. Koch, M. Downing, and L. Litvak, "Current steering creates additional pitch percepts in adult cochlear implant recipients," *Otology and Neurotology*, 28:629-636, 2007.

[13] C. K. Berenstein, L. H. M. Mens, J. J. S. Mulderr, and F. J. Vanpouke, "Current steering and current focusing in cochlear implants: Comparison of monopolar, tripolar and virtual channel electrode configurations," *Ear & Hearing*, 29(2):250-260, 2008.

[14] F. Rattay, “Analysis of models for external stimulation of axons,” *IEEE Transactions on Biomedical Engineering*, 33(10):974-977, Oct 1986.

[15] L. Tung, “Chapter 2.3: The generalized activating function”, I. R. Efimov, M. W. Kroll, and P. J. Tchou (Eds.), *Cardiac Bioelectric Therapy: Mechanisms and Practical Implications.* Springer Science + Business Media, LLC: New York, New York (2009).

[16] C. T. M. Choi and C. Hsu, “Conditions for Generating Virtual Channels in Cochlear Prosthesis Systems,” *Annals of Biomedical Engineering*. 37(3):614-624, March 2009.

[17] L. M. Litvak, A. J. Spahr, and G. Emadi, “Loudness growth observed under partially tripolar stimulation: Model and data from cochlear implant listeners,” *Journal of Acoustical Society of America*. 122(2): 967-981, August 2007.

[18] D. Greenwood, “A cochlear frequency-position function for several species – 29 years later,” *Journal of Acoustical Society of America*, 87(6): 2592-2605, June 1990.

[19] O. Stakhovskaya, D. Sridhar, B. H. Bonham, and P. A. Leake, “Frequency map for the human cochlear spiral ganglion: implications for cochlear implants,” *Journal of the Association for Research in Otolaryngology*, 8(2): 220-233, June 2007.

[20] J. Frijns, R. Kalkman, F. Vanpoucke, J. Bongers, and J. Briare, “Simultaneous and non-simultaneous dual electrode stimulation in cochlear implants: evidence for two neural response modalities,” *Acta Oto-Larngologica*, 129: 433-439, 2009.

[21] Y. Xu and L. M. Collins, “Threshold prediction for noise-modulated electrical stimuli using a stochastic auditory nerve model: Implications for cochlear implants,” *IEEE International Conference on Acoustics, Speech and Signal Processing – Proceedings,* 2: II/1929-II/1932, 2002.

[22] P. T. Bhatti, *A high-density thin-film electrode array for cochlear prosthesis*, Published PhD Thesis, University of Michigan, 2006.

[23] J. Laforet, J. D. Falcone, N. Veau, and D. Guiraud “Gom2n : A Software to Simulate Multipolar Neural Stimulation for Cochlear Implants,” *5th International IEEE EMBS Conference on Neural Engineering,* Cancun, Mexico, April 2011.

[24] K. IversonP. T. Bhatti, , J. D. Falcone , and B. R. McKinnon, “Cochlear Implantation Using Thin Film Array Electrodes,” *Otolaryngology-Head and Neck Surgery Journal*, to be published.

[25] P. Wardrop, D. Whinney, S. J. Rebscher, J. T. Roland Jr., W. Luxford, and P. A. Leake, “A temporal bone study of insertion trauma and intracochlear position of cochlear implant electrodes. I: Comparison of Nucleus banded and Nucleus *Contour*™ electrodes,” *Hearing Research,*203 (1-2): 54-67, May 2005.

[26] P. Wardrop, D. Whinney, S. J. Rebscher, W. Luxford, and P. A. Leake, “A temporal bone study of insertion trauma and intracochlear position of cochlear implant electrodes. II: Comparison of *Spiral Clarion*™ and *HiFocus II*™ electrodes,” *Hearing Research*, 203 (1-2): 68-79, May 2005.

[27] D. R. Ketten, M. W. Skinner, G. Wang, M. W. Vannier, G. A. Gates, and J. G. Neely, “In vivo measures of cochlear length and insertion depth of nucleus cochlear implant electrode arrays”, *Annals of Otology, Rhinology, and Laryngology*, 107: 1-16, 1998.

[28] Stefan B. Nielsen, M.Sc., R&D Engineer, MED-EL, Personal Interview, Feb. 16, 2011.